Probing non-covalent interactions with a second generation energy decomposition analysis using absolutely localized molecular orbitals

Paul R. Horn,[1, a)] Yuezhi Mao,[1] and Martin Head-Gordon[1, b)]
Kenneth S. Pitzer Center for Theoretical Chemistry, Department of Chemistry, University of California, Berkeley, CA 94720 and Chemical Sciences Division Lawrence Berkeley National Laboratory Berkeley, CA, 94720 Phone: 510-642-5957 Fax: 510-643-1255

An Energy Decomposition Analysis (EDA) separates a calculated interaction energy into as many interpretable contributions as possible; for instance, permanent and induced electrostatics, Pauli repulsions, dispersion and charge transfer. The challenge is to construct satisfactory definitions of all terms in the chemically relevant regime where fragment densities overlap, rendering unique definitions impossible. Towards this goal, we present an improved EDA for Kohn-Sham density functional theory (DFT) with properties that have previously not been simultaneously attained. Building on the absolutely localized molecular orbital (ALMO)-EDA, this second generation ALMO-EDA is variational and employs valid antisymmetric electronic wavefunctions to produce all five contributions listed above. These contributions moreover all have non-trivial complete basis set limits. We apply the EDA to the water dimer, the T-shaped and parallel-displaced benzene dimer, the *p*-biphthalate dimer "anti-electrostatic" hydrogen bonding complex, the biologically relevant binding of adenine and thymine in stacked and hydrogen-bonded configurations, the triply hydrogen-bonded guanine-cytosine complex, the interaction of Cl^- with s-triazine and with the 1,3-dimethyl imidazolium cation, which is relevant to the study of ionic liquids, and the water formaldehyde vinyl alcohol ter-molecular radical cationic complex formed in the dissociative photoionization of glycerol.

I. INTRODUCTION

Energy decomposition analysis (EDA) methods are tools for understanding the physical contributions that give rise to often nuanced intermolecular (or intramolecular) interactions computed in molecular orbital (MO) calculations using density functional theory (DFT) or other electronic structure methods. A well-designed EDA can reveal chemically useful information that can guide future investigations or shed light on a surprising result. The terms in an EDA, such as permanent electrostatics (ELEC), polarization (POL), charge transfer (CT), Pauli repulsions (PAULI), and dispersion (DISP), correspond to immensely useful physical concepts that chemists often appeal to in order to explain their findings. However, the relative importance of each of these effects is not always clear from back-of-the-envelope calculations. It is the goal of an EDA to associate with each of these chemical concepts a concrete numerical value describing its contribution to the intermolecular interaction of interest.

Unfortunately, the physical concepts that chemists use to make sense of intermolecular systems do not have unique definitions in the chemically interesting overlapping regime. Due to this non-uniqueness, many methods have been developed[1] to perform EDA, which vary both in their level of description of the interactions and in their formal properties. In light of the non-uniqueness, it is important to develop EDA methods that have as many good formal properties as possible; for example those listed recently[2]. We will focus on this challenge for EDA based on density functional theory (DFT), the most widely used electronic structure method. DFT is capable of good accuracy for the treatment of many intermolecular interactions[3–6], thanks to the development of damped C_6 potentials[7,8], non-local correlation (NLC) functionals[9,10] and functionals that are optimized to include such components[11–14].

The Kitaura-Morokuma (KM)-EDA[15–17] is one of the oldest EDA methods and divides the interaction energy of a cluster of monomers into electrostatic, exchange repulsion, polarization, charge transfer, and unascribable, mixed interaction components. The electrostatic and polarization terms are both defined using electronic wavefunctions that are not properly antisymmetric, leading to potentially unphysical terms. This method also depends on an atomic orbital (AO) basis partitioning to separate polarization and charge transfer.

The EDA method originally proposed by Ziegler and Rauk[18–20] and further generalized by others[21–23] divides the DFT interaction energy into electro-

[a)]Electronic mail: prhorn@berkeley.edu
[b)]Electronic mail: mhg@cchem.berkeley.edu

static, Pauli, and orbital contributions. Contained unseparated within the orbital term are all contributions from wavefunction relaxation, which other schemes associate with CT and POL. As in KM-EDA, the electrostatic interaction is evaluated as the classical Coulomb interaction between monomer charge distributions computed in isolation and translated to the monomer positions in the cluster geometry. The Pauli repulsion term in this method furthermore does not have a definite sign, so it can be attractive for some model chemistries (e.g. functionals that account for dispersion without an obviously separable dispersion correction term), since it may include dispersion.

The absolutely localized MO (ALMO)-EDA[24–26] and block-localized wavefunction (BLW)-EDA[27–30] methods rely on fragment-blocking the AO-to-MO coefficient matrix[31–33] to separate POL from CT and also compute a frozen orbital interaction term evaluated with a wavefunction formed from the MOs of isolated fragments. The ALMO-EDA has also been extended to wavefunction-based correlation at the level of second-order Møller-Plesset perturbation theory (MP2)[34]. While separating POL and CT is desirable, the constraint of fragment-blocking has typically been imposed by using AO basis sets; an approach that lacks a meaningful complete basis set (CBS) limit.[2,35,36] A separation of the frozen orbital interaction into classical electrostatic and Pauli repulsion contributions (as well as a dispersion contribution if the form of the exchange-correlation functional permits it)[30] can be performed in BLW-EDA just as it is performed in the generalized Ziegler-Rauk approach[21–23]. This separation is explicitly avoided in the original ALMO-EDA due to the improper treatment of electron antisymmetry in such decompositions (despite the potential for greater descriptive power in at least some circumstances).

The density-based EDA (DEDA)[37,38] also decomposes an interaction energy into frozen, polarization, and charge transfer contributions. Unlike the ALMO and BLW EDAs, a portion of real space instead of the AO basis space is ascribed to each monomer to define the separation of CT from POL. This choice yields a well-defined CBS limit (at the price of a new dependence on grid partitioning), but also changes the physical content of the POL and CT terms. In DEDA, wavefunction relaxations that delocalize electrons between monomers contribute to POL provided that they do not cause a *net* flow of charge between the monomers, while these relaxations are part of CT in the ALMO and BLW-EDAs[2]. Řezáč and de la Lande[39] similarly employ constrained DFT to analyze the charge transfer contributions to interaction energies. The frozen term in DEDA is also redefined because the monomer MOs are not frozen but instead are allowed to relax subject to the constraint of a frozen density. The separation of this "constant density" frozen energy into electrostatic and Pauli repulsion terms is also possible, and, by construction, the electrostatic contribution is computed with valid antisymmetric electronic wavefunctions. However, we have shown[40] that much of the energy lowering in the frozen density wavefunction optimization is associated with the delocalization of electrons across monomers (i.e. arguably CT in character). Such a treatment may be beneficial in the construction of force fields, which lack explicit CT terms, but its utility for the identification of physical contributions to quantum-mechanical interaction energies is questionable.

The Natural EDA (NEDA)[41–43] decomposes an interaction energy into contributions from electrostatics, polarization, charge transfer, a self-energy term, and a core term describing Pauli repulsion and exchange-correlation effects. Separation of permanent electrostatics from polarization depends on the same calculation of classical electrostatic interactions between monomer charge distributions described above. Unlike the above methods that separate a charge transfer component, NEDA is not variational due to its dependence on the natural bond orbital (NBO)[44,45] procedure to identify polarized monomer Lewis-like determinants in the supersystem wavefunction. The CT contribution is then identified as all energy lowering from non-Lewis wavefunction components, and it is often computed to be several times larger than the interaction energy itself[43].

Symmetry-adapted perturbation theory (SAPT)[46–53] does not decompose a DFT interaction energy, but rather computes its own perturbative expansion of the interaction energy with an accuracy that depends on the order of perturbation theory and the treatment of monomer wavefunctions. The electrostatic contribution is equivalent to the classical electrostatic interaction of monomers discussed above. The exchange terms enter at all orders of the expansion as corrections to enforce proper antisymmetry of the SAPT wavefunction. Induction, like the orbital term of the generalized Ziegler-Rauk EDA, contains both POL and CT contributions. POL and CT are sometimes separated either by using a partitioning of the one-particle space[52], a scheme which suffers from the same weaknesses as ALMO-EDA and BLW-EDA, or by adding additional potentials to discourage

charge transfer[53]. Recently Lao and Herbert[36] have explored using a constrained-DFT-based definition of charge transfer[37–39] to separate the components of the SAPT induction term without dependence on an AO basis function partitioning.

In this paper, we describe a second generation of the ALMO-EDA for intermolecular interactions and apply the method to several example chemical systems. This advancement was primarily devised to address two weaknesses of the original ALMO-EDA. First, the strong basis set dependence of the POL and CT terms. Second, the minimal descriptive power of a monolithic frozen energy term, which contains contributions from three conceptually distinct terms: electrostatics, Pauli repulsion, and dispersion. The definitions of these modified terms are discussed in the following section on Theory. Ultimately, decomposition schemes must be judged by their utility in elucidating chemical phenomena. To this end, we apply our new EDA scheme to the description of interactions in several chemically interesting examples. These examples are as follows: the "anti-electrostatic" hydrogen bonds (between two anions) which has recently been controversial[54–56], Watson-Crick (hydrogen-bonded) versus stacked complexes of adenine and thymine[57], the interactions between chloride anion and the 1,3-dimethyl imidazolium cation[58], and finally the intermolecular interactions in a ter-molecular complex that is involved in the photoionization mass spectrometry of glycerol[59].

II. THEORY

The ALMO-EDA decomposes the intermolecular interaction energy, $\Delta E_{\rm INT}$, at a particular geometry into three further interactions, a frozen component, $\Delta E_{\rm FRZ}$, a polarization effect, $\Delta E_{\rm POL}$, and a charge transfer contribution, $\Delta E_{\rm CT}$

$$\Delta E_{\rm INT} = E_{\rm FULL} - \sum_F E_F \tag{1}$$

$$= \Delta E_{\rm FRZ} + \Delta E_{\rm POL} + \Delta E_{\rm CT} \tag{2}$$

In Eq. (2), both the complex and the isolated fragments, F, are treated at the geometry of the complex. This means we will not track changes in geometry. If one wants to do so, one adds to $\Delta E_{\rm INT}$ the positive semi-definite "geometric distortion" (GD) energy for deforming each fragment, F, from its optimal isolated geometry to the complex geometry:

$$\Delta E_{\rm GD} = \sum_F E_F - E_F^{(F)} \tag{3}$$

The first intermediate energy of the complex, the frozen energy, $E_{\rm FRZ} = E\left(\mathbf{P}_{\rm FRZ}\right)$, is obtained with constraints on the orbitals (or density matrix) to prevent polarization and charge transfer. The difference between this energy and the energy of the fragments defines the frozen interaction introduced above, $\Delta E_{\rm FRZ}$. Physically, $\Delta E_{\rm FRZ}$ contains the three contributions which arise without any relaxation of the fragment orbitals: attractive dispersion (DISP) interactions, Pauli repulsion (PAULI) and permanent electrostatics (ELEC). Separating only the DISP component isolates a "dispersion-free" frozen interaction, $\Delta E_{\rm FRZ\_DF}$, which is the sum of PAULI and ELEC (these terms are both large in the overlapping regime and sometimes significantly cancel each other). Thus we may summarize:

$$\Delta E_{\rm FRZ} = E_{\rm FRZ} - \sum_F E_F \tag{4}$$

$$= \Delta E_{\rm DISP} + \Delta E_{\rm FRZ\_DF} \tag{5}$$

$$= \Delta E_{\rm DISP} + \Delta E_{\rm PAULI} + \Delta E_{\rm ELEC} \tag{6}$$

There are two significant changes in the treatment of the frozen interaction energy in our new ALMO-EDA relative to the earlier version. The first change is that the initial or frozen supersystem wavefunction, which yields the frozen energy, can be relaxed subject to the constraints of constant 3-space density (no polarization) and no CT. This refinement of the initial supersystem wavefunction can be considerable when Pauli repulsions are very strong (such as for chemical bond formation)[40]. However, it is usually not necessary for intermolecular interactions for which the relaxation under these constraints lowers the energy of the initial supersystem wavefunction only minimally[40].

The second and most important change to FRZ is that we compute an energetically optimal orthogonal fragment decomposition[60] of the frozen wavefunction of the complex in order to define the DISP, PAULI and ELEC components (and FRZ_DF if desired). In brief, this is accomplished by minimizing the kinetic energy pressure contribution to the Pauli repulsion energy, $T_{\rm KEP}$ (defined below), to define sets of fragment-localized orthogonal orbitals, that partition the frozen density matrix into a sum of fragment contributions, $\mathbf{P}_{\rm FRZ} = \sum_F \tilde{\mathbf{P}}_F$. The tildes indicate that these fragment density matrices, and the corresponding densities, $\tilde{\rho}_F$, are modified from the isolated fragment quantities, $\mathbf{P}_F$ and ρ_F. The "kinetic energy pressure" is defined by constrained minimization of:

$$T_{\rm KEP} = \sum_F E_F[\tilde{\mathbf{P}}_F] - E_F[\mathbf{P}_F] \tag{7}$$

with respect to $\tilde{\mathbf{P}}_F$. Its minimization yields the smallest increase in the sum of isolated fragment energies that can be obtained subject to the constraint of frozen density partitioning.

These fragment densities are first used to evaluate the permanent electrostatics, ELEC. $\Delta E_{\rm ELEC}$ describes the contribution from the Coulomb interaction between fragment charge distributions to binding and is evaluated using the modified fragment densities (after adding in the fragment nuclear charges: $\tilde{\rho}_F^{tot}(\mathbf{r}) = \tilde{\rho}_F(\mathbf{r}) + \rho_F^{nuc}(\mathbf{r})$):

$$\Delta E_{\rm ELEC} = \sum_{F<G} \iint d\mathbf{r}_1 d\mathbf{r}_2 \tilde{\rho}_F^{tot}(\mathbf{r}_1) r_{12}^{-1} \tilde{\rho}_G^{tot}(\mathbf{r}_2) \quad (8)$$

This definition is an alternative to the commonly employed classical definition, CLS_ELEC, which simply uses the total densities of the isolated fragments, $\rho_F^{tot}(\mathbf{r})$ in Eq. (8). CLS_ELEC is less than ideal because the sum of the isolated fragment densities does not add up to the frozen density in the overlapping regime. This means that, while easy to compute, the electrostatic interaction by the classical definition computes the coulomb interaction between electrons in a charge distribution that is not adopted in the initial state and moreover could potentially never exist within the given model chemistry. The two definitions agree in the non-overlapping regime but can differ significantly at short range, as the modified densities deform according to the overlap of the fragment orbitals[60].

The modified fragment densities are also used to evaluate the dispersion term, DISP. $\Delta E_{\rm DISP}$ is intrinsically attractive, and asymptotically decays as R^{-6} between two fragments. It represents the energy lowering due to correlated fluctuations of electrons on two different fragments that is not captured in the mean-field permanent electrostatics term. In the same way as electrostatic interactions can only be interpreted as multipole-multipole interactions in the non-overlapping regime, DISP can likewise only be interpreted as dispersion in the non-overlapping regime. In the overlapping regime, DISP corresponds to "dispersive" interfragment exchange-correlation effects that smoothly change into true dispersion as overlap decreases.

In our EDA, DISP is separated from the remainder of interfragment exchange-correlation effects with the help of an auxiliary density functional that is dispersion-free (DF), $E_{xc}^{\rm DF}$. Examples of DF functionals include Hartree-Fock (HF), the so-called dispersionless density functional (dlDF)[61], and revPBE[62]. The optimal choice for $E_{xc}^{\rm DF}$ clearly depends upon the form of E_{xc} itself. For instance, HF may be most appropriate for functionals containing substantial amounts of exact exchange, while revPBE may be most appropriate for functionals without exact exchange. The dispersion energy is naturally defined as that part of the inter-fragment exchange-correlation energy which is captured by E_{xc} but is not captured by $E_{xc}^{\rm DF}$:

$$\Delta E_{\rm DISP} = \left(E_{xc}[\mathbf{P}_{\rm FRZ}] - \sum_F E_{xc}[\tilde{\mathbf{P}}_F] \right) - \left(E_{xc}^{\rm DF}[\mathbf{P}_{\rm FRZ}] - \sum_F E_{xc}^{\rm DF}[\tilde{\mathbf{P}}_F] \right) \quad (9)$$

The reminder of the frozen interaction energy is associated with Pauli repulsion. Pauli repulsion accounts for volume exclusion effects, the dramatic increase in energy observed when two molecules are compressed. Electronic wavefunction antisymmetry requires that electrons of the same spin not occupy the same space, an expression of the Pauli principle, and the repulsive character of this term is a consequence of the increase in kinetic energy associated with decreasing the volume available to each electron due to the presence of all others. An additional consequence of electron antisymmetry is interfragment exchange, which, together with any correlation effects not associated with dispersion, mitigates the volume exclusion effect. These two physical contributions together yield the Pauli repulsion energy in the EDA:

$$\Delta E_{\rm PAULI} = \sum_F \Big(E[\tilde{\mathbf{P}}_F] - E[\mathbf{P}_F] \Big) + \left(E_{xc}^{\rm DF}[\mathbf{P}_{\rm FRZ}] - \sum_F E_{xc}^{\rm DF}[\tilde{\mathbf{P}}_F] \right) \quad (10)$$

The opposite signs of these two contributions to the PAULI term make it formally of indeterminate sign though, for proper choices of the dispersion-free functional (vide infra), the repulsive component dominates.

After $E_{\rm FRZ}$, a second constrained variational calculation is performed to uncover the energy lowering due to polarization (POL). $\Delta E_{\rm POL}$ describes the induced electrostatic interactions resulting from the intra-fragment density relaxation of each monomer in response to all other perturbing monomers in the cluster. Polarization is a response not only to the electric fields produced by other fragments' electrons and nuclei but also, at short inter-fragment separations, to the kinetic energy pressure exerted by the electrons of other fragments due to electronic wavefunction antisymmetry.

This EDA describes polarization using a basis of fragment electric-field response functions (FERFs),[2] which allow each fragment to respond exactly to weak electric fields. The FERF basis is truncated at exact response to a uniform field ($\boldsymbol{\varepsilon}$) and its first derivatives ($\partial\boldsymbol{\varepsilon}/\partial\mathbf{R}$), corresponding to dipolar and quadrupolar responses (FERF-DQ), which is the lowest order that correctly reproduces polarization interactions as inter-monomer overlap approaches zero[2]. The FERF-DQ model provides three dipolar and five quadrupolar polarization functions per occupied MO.

Beginning from the frozen wavefunction, the FERF-DQ subspaces are used in a constrained variational calculation allowing only intra-fragment relaxation (fragment-blocking the DQ-to-MO coefficient matrix) to determine an ALMO-SCF energy, $E_{\text{ALMO-SCF}}$, by solving the "SCF for molecular interactions" (SCF-MI) equations[31,33,63,64] in the FERF-DQ basis. We immediately obtain $\Delta E_{\text{POL}} = E_{\text{ALMO-SCF}} - E_{\text{FRZ}}$. The FERF-DQ functions can be constructed from a sufficiently complete basis of any type (e.g. AO's, or plane waves, etc), and the resulting $E_{\text{ALMO-SCF/FERF-DQ}}$ has a meaningful complete basis set limit. This property is an important improvement on the definition of the polarization energy in the previous version of the ALMO-EDA.

Finally, the charge transfer (CT) term, $\Delta E_{\text{CT}} \leq 0$, accounts for donor-acceptor inter-fragment orbital interactions that bring about energy lowering in the system. The energy lowering arises not only from net charge flow between fragments but also by allowing electrons to delocalize across fragments. This term also includes the secondary intra-fragment relaxations that occur in response to the redistribution of charge brought about by these inter-fragment orbital interactions. It is straightforwardly evaluated as the difference between the unconstrained SCF energy and the ALMO-SCF/FERF-DQ energy: $\Delta E_{\text{CT}} = E_{\text{SCF}} - E_{\text{ALMO-SCF/FERF-DQ}}$.

III. RESULTS AND DISCUSSION

A. Computational Details and Validation

Calculations in this work were performed with a standard version of the Q-Chem 4.4 software package[65,66]. The ωB97M-V[14] functional, which includes a VV10[9] non-local correlation functional description of dispersion, is used for all calculations. ωB97M-V is a highly accurate functional for non-covalent interactions[14], and it is therefore ideal for application to EDA of intermolecular interactions. The dispersion-free (DF) functional that is necessary to disentangle dispersion interactions was simply taken as the Hartree-Fock (HF) form, which is appropriate for a range-separated hybrid functional such as ωB97M-V[60]. The large def2-QZVPPD[67] basis was used to compute all the interaction energies (without counterpoise correction) and their decompositions in this work, so that all results are fairly close to the CBS limit.

Polarization subspaces are FERF-nDQ[2] unless otherwise stated. We also use the antisymmetric product of monomer wavefunctions as the initial supersystem wavefunction throughout this work. Optimization of the initial supersystem wavefunction is unnecessary for the intermolecular interactions that we will examine, although this relaxation has been shown to be significant in the context of breaking covalent bonds.[40] Many of the structures come from other works and will be described in turn. Images of molecular structures were generated with the help of IQmol.

We note that the resultant energy components of an EDA are inevitably functional-dependent. Nonetheless, this new EDA method is able to produce reasonable results as long as functionals that can accurately describe non-covalent interactions are employed and an appropriately paired DF functional is chosen. As a brief validation, EDA results for three prototypical non-covalent complexes from the S22[57] dataset are shown in Table I as computed using three functionals that are suitable for non-covalent interactions. In addition to ωB97M-V (used for all reported results), we compare to the pure B97M-V functional[13] (using revPBE as the DF functional), and the conventional B3LYP-D3 (0) hybrid[8,68–70] (using HF as the DF functional).

For each system, no significant changes can be seen in the resulting energy components when different functionals are employed, keeping in mind the discrepancy in total interaction energies and the fact that dispersion corrections are incorporated differently in these functionals. This validation provides support for drawing chemical conclusions from the results using just a single functional later. For the water dimer, CT is roughly 38-42% of the total interaction energy, a bit smaller than results obtained[71] with the first generation ALMO-EDA, where POL is slightly contaminated[2,35] with CT. It is also interesting to see that DISP accounts for almost all of the FRZ binding energy. The two different conformers of benzene dimer show the expected large difference in DISP, which is far more important for the stacked conformer.

TABLE I: EDA results (in kJ/mol) for three prototypical complexes in the S22 dataset: water dimer ("hydrogen bonded"), and benzene dimer in T-shaped ("mixed") and parallel-displaced ("dispersion-dominated") configurations. Total interaction energies and energy breakdowns are evaluated with three functionals (ωB97M-V, B97M-V, B3LYP-D3 (0)) using the def2-QZVPPD basis. As recommended in Sec. II, Hartree-Fock is chosen as the DF functional for ωB97M-V and B3LYP-D3 (0), while revPBE is employed for B97M-V. The reference values for the interaction energies of these systems are -20.87, -11.37, and -11.10 kJ/mol, respectively.[72]

	Water Dimer			Benzene Dimer (T-shaped)			Benzene Dimer (parallel-displaced)		
	ωB97M-V	B97M-V	B3LYP-D3 (0)	ωB97M-V	B97M-V	B3LYP-D3 (0)	ωB97M-V	B97M-V	B3LYP-D3 (0)
ELEC	-65.75	-62.77	-66.10	-21.39	-19.94	-20.68	-34.04	-32.22	-33.47
PAULI	65.02	61.66	65.40	31.82	31.24	30.68	59.35	56.70	56.63
DISP	-7.66	-6.80	-8.02	-17.85	-16.69	-17.35	-32.53	-29.88	-27.81
FRZ	-8.38	-7.91	-8.73	-7.42	-5.39	-7.35	-7.21	-5.40	-4.65
POL	-4.61	-4.37	-4.46	-1.43	-1.29	-1.11	-1.59	-1.51	-1.17
CT	-7.74	-8.67	-8.80	-2.47	-3.28	-3.11	-3.21	-4.00	-4.20
INT	-20.74	-20.95	-21.99	-11.32	-9.96	-11.57	-12.02	-10.90	-10.02

B. Anti-Electrostatic Hydrogen Bonding

The first system that we investigate is the *p*-biphthalate dimer, one of the several controversial[54–56] anti-electrostatic hydrogen bonding interactions. In terms of structure (Figure 1), the optimized dimer exhibits relatively normal hydrogen bonding motifs, but both monomers are anions, and the stationary points identified along the dissociation coordinate are higher in energy than the isolated monomers due to these net charges. The computational finding of local minima in the anion-anion complex is surely correct, and indeed experimental evidence is emerging for stable cation-cation complexes in either the solid state[73] or in ionic liquids[74].

The primary issue is the origin of the binding, and thus the nature of the hydrogen bond. This "anti-electrostatic" interaction is seen by Weinhold and Klein[54] (WK) as an indicator of the profound importance of quantum-mechanical (i.e. donor-acceptor) orbital interactions in hydrogen bonding complexes[75]. By contrast, the simplest electrostatic model of charge-charge repulsion would suggest a purely repulsive interaction. However, this interpretation is inevitably controversial[55,76], because it ignores other electrostatic effects like favorable permanent charge-dipole and dipole-dipole interactions, the stabilization owing to interpenetration of fragment charge distributions, as well as induced electrostatics (i.e. POL). Our new ALMO-EDA is a suitably unbiased tool with which to examine these neglected effects, as it is based on the variational principle combined with physically well-founded constraints.

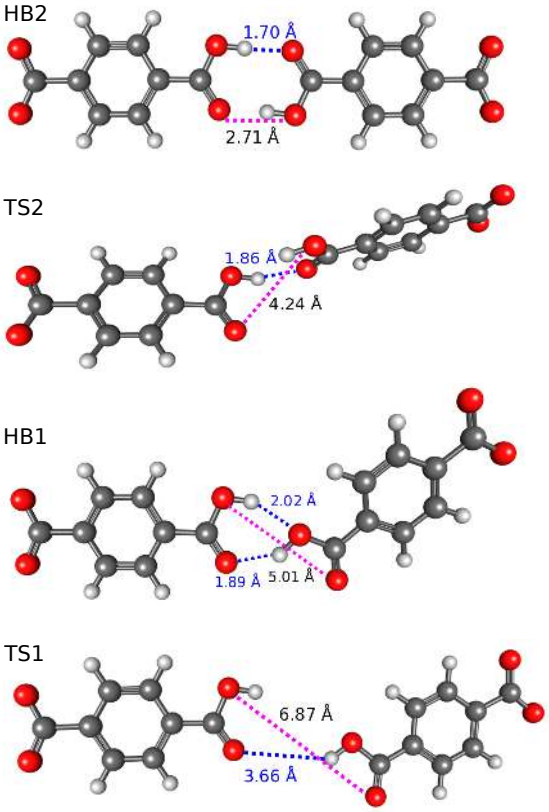

FIG. 1: Structures at minima (HB2 and HB1) and transition states (TS2 and TS1) for the dissociation of the *p*-biphthalate di-anionic dimer as given by WK[54]. The dotted magenta lines indicate the maximum O$\cdots$O distances between the two carboxyl groups in contact with each other.

We take the two hydrogen-bonding minima (HB1 and HB2) and transition state structures (TS1 and TS2) from WK, unmodified, for direct comparison (Figure 1). The binding energies (Figure 2(a)) are quite similar to those presented previously despite the change in model chemistry, and the relative energetics are well described by changes in the interaction energies alone, allowing us to largely neglect geometric distortions in this analysis.

Because our EDA scheme shares a common intermediate state, the initial supersystem wavefunction, with the generalized Ziegler-Rauk EDA employed by Frenking and Caramori[55] (FC) to analyze another anti-electrostatic hydrogen bonding complex, we will discuss the results of this scheme as well as our own. Their approach includes three terms that sum to the interaction energy, ΔE_{Coul}, ΔE_{Pauli}, and ΔE_{Orb}, which we will refer to as CLS_ELEC, CLS_PAULI, and ORB respectively.

We first address the question of why there is a minimum at all. The interaction energy for TS1, the final barrier to dissociation, is described almost entirely by the electrostatic term (ELEC) with negligible contributions from other terms (Figure 2(b)). The electrostatic term at this separation is moreover almost identical to the analogous CLS_ELEC term due to weakly overlapping fragments (Figure 3(b)). We infer that it is dominated by the repulsive monopole-monopole interaction as the monopole-dipole couplings will be attractive. Past TS1, the interaction energy decays because of the decrease in this unfavorable electrostatic interaction with increasing inter-monomer distance.

At closer separations than TS1, ELEC, DISP, POL, and CT all become more favorable, and only the PAULI term becomes more repulsive due to increased inter-fragment overlap. All favorable terms follow the same energetic ordering as the interaction energy itself, and the Pauli repulsion term progresses in the opposite way. According to our new EDA, formation of the hydrogen bonds in this dianionic system is quite similar to a conventional hydrogen bond: permanent electrostatics, induced electrostatics, dispersion and orbital interactions all become more favorable on closer approach, counterbalanced by Pauli repulsion becoming strongly repulsive. Overall, the hydrogen bond is the net result of a delicate balance between these interactions, rather than simply reflecting donor-acceptor (CT) effects as argued by WK[54] without the benefit of the present decomposition.

Concerning permanent electrostatics, we note from Figure 3(b) that both ELEC and CLS_ELEC are *net attractive* at HB2. Hence *by either definition* of permanent electrostatics, this most stable structure is not "anti-electrostatic" in character after all! Our new definition, ELEC, is more attractive than the classical definition, CLS_ELEC, because of overlap-induced changes in the fragment density. To understand this effect, we consider Fig-

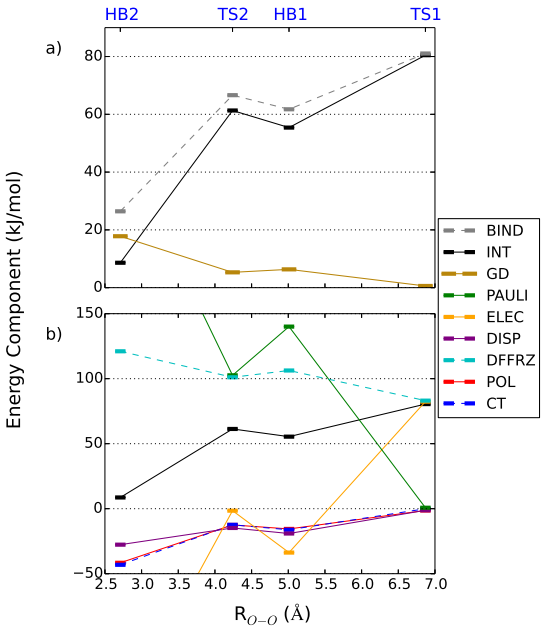

FIG. 2: Energies in kJ/mol relative to dissociated monomers, (a), and the associated EDAs, (b), for the *p*-biphthalate dimer dissociation coordinate minima (HB2 $R_{O\text{-}O}$ = 2.71 Å, HB1 $R_{O\text{-}O}$ = 5.01 Å) and transition structures (TS2 $R_{O\text{-}O}$ = 4.24 Å, TS1 $R_{O\text{-}O}$ = 6.87 Å) as given by WK[54], where $R_{O\text{-}O}$ denotes the maximum O$\cdots$O distance between the two contacting carboxyl groups (indicated by the dotted magenta lines in Figure 1). At each of the four stationary points, the y value of each level indicates the magnitude of the various energy components. Note that the lines connecting these levels serve only to guide the eye. Part (a) shows that geometric distortion (GD) does not qualitatively affect the relative values of overall binding (BIND), which justifies decomposition in (b) of the interaction energy (INT) into electrostatic (ELEC), Pauli repulsion (PAULI), dispersion (DISP), polarization (POL), and charge transfer (CT) contributions. The sum of PAULI and ELEC, the dispersion-free frozen energy (DFFRZ), is also plotted.

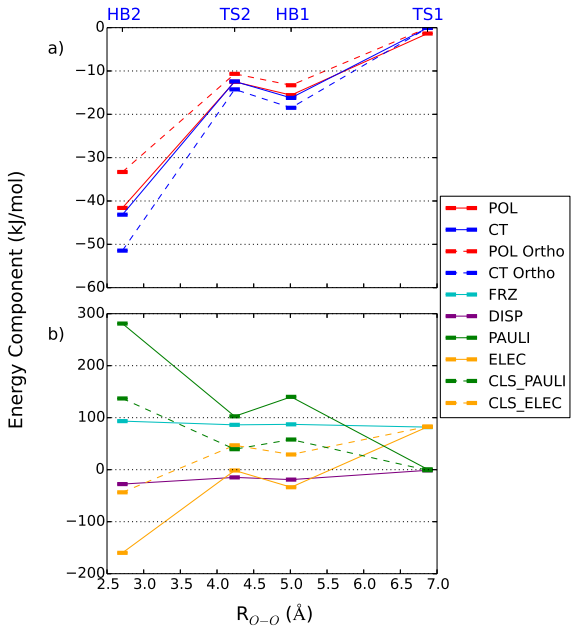

FIG. 3: Results for different choices in EDA term definitions computed for the *p*-biphthalate structures (in kJ/mol) presented in the same format as in Figure 2. Part (a) compares the effect of using orthogonalized (ortho) FERFs versus the standard option of not orthogonalizing, showing that the differences are relatively small (largest for HB2) and do not alter the qualitative description of the interaction. Part (b) compares results for the decomposition of the frozen orbital energy (FRZ), which is nearly unchanged across the four structures, by the scheme used in this work (ELEC, PAULI, DISP) and that used in generalized Ziegler-Rauk EDA[18,19,21–23] (CLS_ELEC, CLS_PAULI) as employed by FC[55].

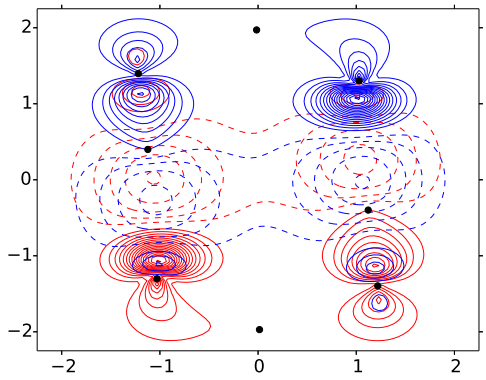

FIG. 4: Contour plot of the change in density for the two (Red and Blue) p-biphthalate monomers in the HB2 complex of WK[54] with inter-fragment hydrogen bond lengths of $R_{O\text{-}H}$ = 1.70 Å. Values plotted are the differences in the 3-space total spinless density, integrated to a plane ($\Delta_A(x,y) = \int dz \Delta\rho_A(x,y,z)$), for each fragment, A, upon going from the optimal isolated fragment density matrix to that assigned to the fragment within the initial supersystem wavefunction. Contours are evenly spaced at 0.1 $e^-/Å^3$ with positive contours solid and negative contours dashed. Dots indicate the positions of nuclei in the two carboxyl groups (at the top and bottom of the plot) that form the hydrogen bonds. We note the presence of seemingly unavoidable minor orthogonalization tails.

ure 4, which depicts the change in fragment densities at the HB2 structure upon going from those optimal for the fragments in isolation (and used to compute CLS_ELEC) to those assigned to the fragments in the properly antisymmetric initial supersystem wavefunction (and used to compute ELEC). The effect of the antisymmetrization of monomer wavefunctions is, as always, a depletion of charge in the inter-fragment region, which in this case both deshields the hydrogen nuclei and increases density at the oxygen nuclei that are participating in hydrogen bonding. An additional consequence of this antisymmetrization is the inevitable development of small orthogonalization tails near the nuclei of other fragments. The resulting short-range electrostatic interactions are enough to overcome the repulsions between the excess electrons on the anionic fragments that are roughly located on opposite ends of the complex. The additional effects that make CLS_ELEC attractive for HB2 include the attractive interactions between local OH and OC bond dipoles across the hydrogen bond, which decay as R^{-3} with monomer separation distance and the classically permitted interpenetration of fragment charge densities.

Bringing the anion monomers together to finally form HB2 via TS2 from HB1, which is accessed from TS1, leads to increasingly unfavorable Pauli repulsion contributions for HB1 and HB2. The sum of ELEC, PAULI, and DISP is the frozen orbital (FRZ) interaction. Despite the large changes in electrostatic and Pauli repulsion terms across the coordinate, FRZ is, perhaps surprisingly, nearly constant at each of the four structures (Figure 3(b)). Thus

energetic benefits in ELEC and DISP afforded by shorter separations are largely canceled by the concomitant PAULI cost. The frozen orbital interaction is equivalent to the sum of CLS_ELEC and CLS_PAULI in generalized Ziegler-Rauk EDA.

The remaining portion of the interaction energy is derived from intra-fragment polarization (POL) and inter-fragment charge transfer (CT). These contributions (which sum to the ORB term discussed by FC) have roughly the same energetic significance in each of the structures considered, as can be seen in Figures 2(b) and 3(a). Comparison of POL and CT is of interest because WK emphasized the importance of inter-fragment donor-acceptor orbital interactions in hydrogen bonded complexes, notably the oxygen lone-pair to OH σ^* charge transfer interaction. Our CT results indeed show important contributions from inter-fragment electron delocalization, and this likely plays an important role in determining the details of the fragment orientations in HB1 and HB2 due to the directional nature of orbital interactions. However, the closer contacts needed for stronger inter-fragment donor-acceptor interactions cannot occur to the same degree without increasing polarization (POL) to allow intra-fragment relaxation that relieves the perturbation due to the other fragments. Our results in Figures 2(b) and 3(a) show that POL, like CT, is also increasingly stabilizing as the fragments are brought together. We find this unsurprising: for an interaction involving monomers with net charges and local dipoles, induced electrostatic effects should play a significant role.

Weinhold has argued[77] that POL may be greatly overestimated by treatments involving nonorthogonal one-particle spaces, as we have used here. While we have reported results[2] showing that this is not the case for our FERF-nDQ model, we also include results for another polarization model (Figure 3(a)) that employs subspaces produced by an energetically cognizant orthogonalization[2] of these same non-orthogonal subspaces. The differences between the two sets of results for polarization and charge transfer systematically enhances the CT:POL ratio from roughly 1:1 without orthogonalization to roughly 3:2 for the HB1 and HB2 structures (it changes somewhat less for TS1 and TS2). The two POL curves can be viewed as upper and lower estimates of the polarization contribution. Using the orthogonalized results does not influence the qualitative interpretation of the interaction discussed above.

In summary, the position[54] that charge-transfer (CT) or resonance effects are absolutely dominant in hydrogen bonding in the *p*-biphthalate dimer dianion is *not* supported by analysis with the new EDA. Instead a more nuanced picture emerges from Figures 2 and 3. CT *does* make an important contribution to binding, but polarization (POL) is close behind. The effects of these two terms are synergistic, as the molecular complex can substantially lower its energy by polarizing fragments that are in close proximity to another molecule, and this close proximity is necessary for strong orbital interactions. Likewise, the dispersion energy (DISP) becomes stronger at close separations, and also contributes to stabilizing of the hydrogen-bonded structures. Finally, at the most stable HB2 structure, the hydrogen bonds are *not* anti-electrostatic. The monopole-based caricature ignores stabilizing contributions from favorable local multipolar interactions and fragment charge interpenetration which contribute to the attractive permanent electrostatics evaluated either quasi-classically (CLS_ELEC), or quantum mechanically via the ELEC term of the new EDA.

C. DNA base pairs

We now turn to the biologically relevant interactions between adenine and thymine (A$\cdots$T) base pairs with the aim of characterizing the qualitative differences between the Watson-Crick and stacked conformations (Figure 5) of this system taken from the S22[57] dataset. The EDA results for these two interaction energies appear in Table II.

Unlike in the more similar set of structures investigated above, the more strongly bound complex does not simply have all attractive terms more favorable than those of the less strongly bound complex. In particular, the DISP term, which is the contribution to binding from dispersive interactions, is more than twice as favorable for the stacked complex than for the Watson-Crick complex, due to the larger number of inter-fragment contacts in the stacked structure. However, the DISP contribution in the Watson-Crick complex is still appreciable due to closer contacts, which, though fewer in number, bring considerable density from the two fragments into close proximity (similar to what we observed in the hydrogen bonds in the previous example).

The Pauli repulsion term in the stacked complex is large and repulsive for a similar reason though not as repulsive as in the Watson-Crick complex where the closer approach of a smaller number of atoms in hydrogen bonding motifs is driven by an increased ability to participate in charge transfer interactions and

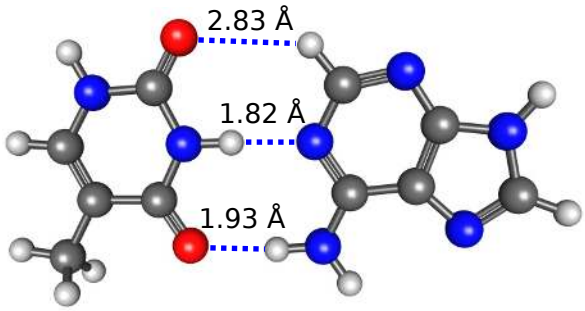

(a) Adenine thymine Watson-Crick structure.

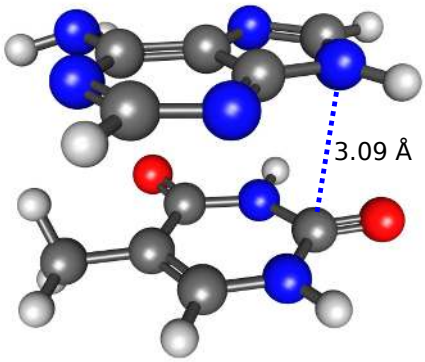

(b) Adenine thymine stacked structure.

FIG. 5: The adenine thymine complex in the hydrogen-bonding Watson-Crick and stacked configurations from the S22[57] dataset with inter-fragment contacts shown. Two hydrogen bonds (1.82 Å and 1.98 Å) are formed in the Watson-Crick complex.

facilitated by increased intra-fragment polarization as well as more favorable electrostatic interactions with deshielded hydrogen atoms. Charge transfer and polarization make only minor contributions to the stabilization of the stacked complex.

In addition, we also investigated the guanine-cytosine (G$\cdots$C) complex in the Watson-Crick configuration (Figure 6), and its EDA results are compared to those for the corresponding A$\cdots$T complex in Table II. While two hydrogen bonds are of roughly the same lengths as in the A$\cdots$T complex, one extra hydrogen bond of even shorter length (1.76 Å) exists in G$\cdots$C, resulting in an ELEC term that is larger by over 50% (about 100 kJ/mol). Although PAULI is also considerably more repulsive (by 80 kJ/mol) due to the formation the third hydrogen bond, it is outweighed by more stabilizing ELEC and DISP, which result in a much more favorable FRZ

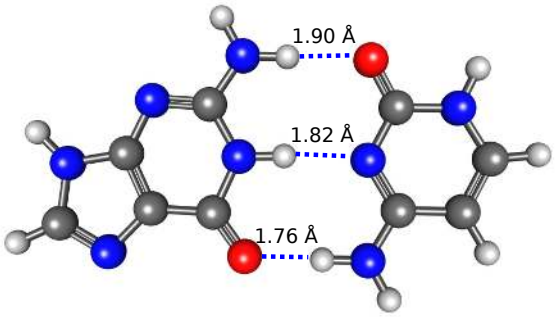

FIG. 6: The guanine-cytosine complex in the hydrogen-bonding Watson-Crick configuration with inter-fragment contacts (three hydrogen bonds) shown. The geometry is optimized at the ωB97M-V/def2-TZVPPD level of theory.

term (-35 kJ/mol vs. -8 kJ/mol in A$\cdots$T). The other two synergistic components (POL and CT) are also considerably larger in the G$\cdots$C complex, which is especially true for POL whose contribution is almost doubled. Overall, although only one extra hydrogen bond is formed in the G$\cdots$C complex, the magnitude of the total interaction energy increases by almost two-fold compared to that of A$\cdots$T (Watson-Crick), and this "non-linear" enhancement of binding is a result of the concerted stabilizing effect of the four favorable components (ELEC, POL, CT, and DISP).

Let us consider the classical decomposition of the frozen interaction, FRZ, which is given in Table II as CLS_ELEC and CLS_PAULI. FRZ is more favorable in the stacked structure, which hints at increased dispersion and decreased Pauli repulsions. However, CLS_PAULI is very small in the stacked structure, leaving CLS_ELEC as the only term large enough to account for the interaction energy. Without prior knowledge of this system, the classical decomposition may lead one to believe that the interaction is almost entirely electrostatic in character instead of containing a large dispersive contribution. In fact, the dispersion is at least partly included in CLS_PAULI, disguising its effect in the classical decomposition. Care should thus be taken in interpreting results of the classical decomposition when modern density functionals capable of describing dispersion are employed. This confusion is eliminated in the new EDA via the DISP term, as discussed previously.

	adenine-thymine		guanine-cytosine
	H-bonded	Stacked	H-bonded
CLS_ELEC	-113.56	-47.85	-181.76
CLS_PAULI	105.40	12.13	146.70
ELEC	-185.41	-104.71	-284.78
PAULI	207.69	135.00	289.00
DISP	-30.44	-66.02	-39.28
FRZ	-8.16	-35.72	-35.06
POL	-24.88	-7.80	-50.54
CT	-33.68	-7.70	-45.59
INT	-66.71	-51.23	-130.69

TABLE II: Energy decomposition analysis results in kJ/mol for the interaction of adenine with thymine in the Watson-Crick and stacked configurations with corresponding structures taken from the S22[57] dataset, and for the interaction between guanine and cytosine in a Waston-Crick complex (whose geometry is optimized with ωB97M-V/def2-TZVPPD). The shortest inter-fragment heavy-heavy distance in the stacked structure is $R_{C\text{-}N}$ = 3.09 Å. Results for the classical decomposition (FRZ = ELEC + PAULI + DISP = CLS_ELEC + CLS_PAULI) are shown for comparison.

D. Anion-π interactions between Cl^- and 1,3-dimethyl imidazolium and s-triazine

Anion-π interactions are attracting increasing attention[78] as they have become better characterized and as their relevance in contexts ranging from biological macromolecules to ionic liquids has emerged. The interaction of halides with electron-deficient aromatic rings leads to a variety of stable structures depending on the halide and the ring system[79]. For chloride interacting with s-triazine, for instance, there is a planar hydrogen-bonded structure, and a non-planar donor-π acceptor complex, as shown in Figure 7.

Chloride complexes with 1,3-dimethyl imidazolium cation[58,80] (which we will abbreviate as [C_1C_1im]Cl) are relevant to the complex interactions occurring within the corresponding ionic liquids[81]. The [C_1C_1im]Cl dimer exhibits the same motifs seen for chloride-triazine, with a rich range of hydrogen-bonded isomers, and also an out-of-plane donor-π acceptor complex. These optimized structures are also shown in Figure 7. The relative values of the binding energies for different isomers and their origin in the components of the new ALMO-EDA will be the focus of this subsection.

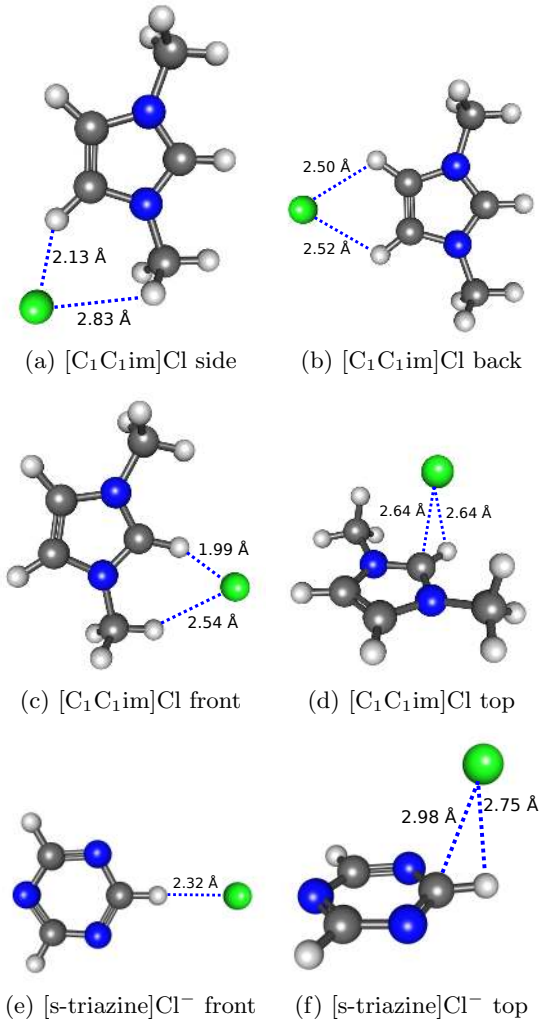

(a) [C_1C_1im]Cl side (b) [C_1C_1im]Cl back

(c) [C_1C_1im]Cl front (d) [C_1C_1im]Cl top

(e) [s-triazine]Cl^- front (f) [s-triazine]Cl^- top

FIG. 7: ωB97M-V/def2-QZVPPD optimized structures for the [C_1C_1im]Cl ion pair and the more weakly bound net anionic [s-triazine]Cl^- system.

The interaction energies and their EDA breakdowns are shown in Table III. Considering the two conformers of [s-triazine]Cl^-, it is evident that the front conformer, which involves a $Cl^- \cdots$H-C interaction, is more stable by about 7 kJ/mol. The principal origin of the difference is a more favorable frozen interaction (by 7 kJ/mol), which in turn arises primarily from lower Pauli repulsion (by 17 kJ/mol). Both conformers exhibit quite similar POL and CT values, with POL being the larger contribution. While both conformers derive the large majority of their binding from POL+CT, the front conformer is able to achieve these comparable orbital interactions with less Pauli repulsion. The non-planar

	[C_1C_1im]Cl				[s-triazine]Cl^-	
	back	side	front	top	front	top
ELEC	-389.38	-430.70	-468.81	-504.61	-72.33	-74.73
PAULI	132.33	177.31	204.36	219.80	77.93	94.83
DISP	-23.38	-27.52	-26.98	-40.04	-12.59	-19.98
FRZ	-280.43	-280.92	-291.44	-324.84	-6.99	0.12
POL	-37.21	-48.59	-61.42	-49.68	-21.83	-20.99
CT	-19.70	-32.11	-48.81	-42.45	-13.39	-14.43
INT	-337.34	-361.62	-401.67	-416.97	-42.22	-35.30

TABLE III: Energy decomposition analysis of the [C_1C_1im]Cl ion pair and anionic [s-triazine]Cl^- systems in kJ/mol.

donor-π acceptor complex does exhibit a stronger dispersion interaction as might be expected, but this only partially mitigates the larger Pauli repulsion.

The [C_1C_1im]$^+Cl^-$ complexes are vastly more strongly bound than the [s-triazine]Cl^- complexes because of the enormous enhancement in the permanent electrostatics, ELEC, due to the favorable monopole-monopole interaction. As a result, the fragments approach each other more closely, and Pauli repulsions and dispersion are increased in magnitude. The energetic ordering of the classes of structures is also changed relative to the [s-triazine]Cl^- complex. The most stable conformer is the on-top donor-π acceptor structure, which is approximately 15 kJ/mol more stable than the analogous front conformer.

The origin of the change in ordering can be deduced from Table IL, which shows that two synergistic effects (ELEC, DISP) that provide relative stabilization of the top conformer outweigh two synergistic effects (POL, CT) that provide relative stabilization of the front conformer. ELEC is more favorable in the top conformer, overcoming the excess Pauli repulsion to provide a net dispersion-free frozen stabilization of about 20 kJ/mol relative to the front conformer. Thus the more favorable electrostatic interaction between Cl^- and the C_2 site, which holds much of the positive charge, is the single largest driving force. There is also a synergistic enhancement of DISP by about 13 kJ/mol relative to the front conformer, due to the more considerable intermolecular contact and thus stronger dispersion interaction between Cl^- and the π system. By contrast, POL and CT are more favorable in the front conformer, together providing about 18 kJ/mol of net stabilization.

The conclusion that electrostatics play a major role, supported by dispersion interactions, in determining the relative energies of the conformers of the [C_1C_1im]$^+Cl^-$ complexes is broadly consistent with other studies using different density functionals[58,80,81]. Our ωB97M-V calculations are consistent with reported CCSD(T), MP2 and dispersion-corrected B3LYP calculations[58] in predicting that the top conformer is lowest in energy. Finally, the side and back conformers are incrementally less stable than the front conformer. Though ELEC and PAULI vary considerably, the FRZ interaction itself is relatively constant in this set of structures, and the sequence of interaction energies can be largely explained by the trend in POL+CT terms as binding involves presumably more and more electron deficient hydrogens in the progression from back to side to front.

E. Ionized Glycerol Complex

We consider a radical cationic cluster of three fragments (Figure 8) that was identified by Bell et al.[59] as a key intermediate in the dissociative photoionization of glycerol and designated as COM1 in that work. We decompose the interaction energy for this structure, unmodified, by a complete many-body expansion of the interaction energy in Table IV.

A similar analysis was performed in the original work[59] though with a different model chemistry and the older ALMO-EDA, which notably lacks the decomposition of the frozen orbital interaction and the bounded treatment of polarization. As a result of the basis set choice in the earlier study, the change in model chemistry and polarization treatment has little effect on the values of FRZ, POL and CT. The present results therefore largely validate the prior conclusions, as well as providing new insights through the decomposition of FRZ into its ELEC, PAULI and DISP components.

The two-body term between the vinyl alcohol radical cation (A) and water (W), E_2[AW], is the strongest interaction in the many-body expansion. The electrostatic term is large and attractive here as we have seen in other hydrogen bonding systems above; however, in this case there is a favorably aligned monopole-dipole interaction in the absence of a repulsive monopole-monopole interaction. The large, repulsive PAULI term is explained by the short ($R_{O\text{-}H}$ = 1.38 Å) hydrogen bond length between these two monomers, enabling stronger interfragment orbital interactions (CT) as well as favorable permanent (ELEC) and induced (POL) electrostatic interactions with the electron-poor vinyl alcohol radical cation. There is also a less important stabilizing contribution from DISP.

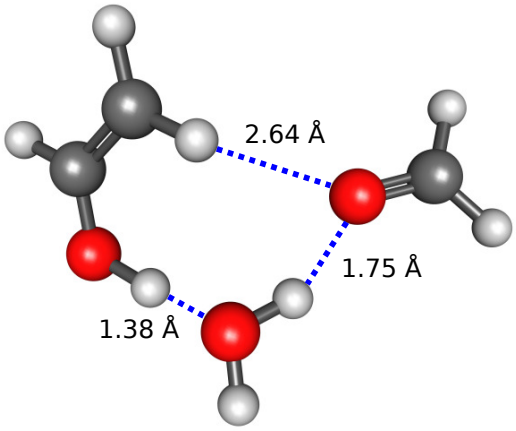

FIG. 8: The COM1 complex from Bell et al.[59] that has been identified as an important intermediate in the dissociative photoionization of glycerol with inter-fragment contacts shown.

	E_2[AW]	E_2[AF]	E_2[WF]	E_3[AWF]	Total[AWF]
ELEC	-215.13	-47.50	-80.76	-1.33	-344.71
PAULI	255.08	10.20	102.13	-0.27	367.14
DISP	-18.38	-4.06	-10.35	0.29	-32.50
FRZ	21.58	-41.36	11.01	-1.31	-10.07
POL	-66.89	-9.14	-7.34	-8.37	-91.74
CT	-70.85	-1.32	-13.50	-5.21	-90.88
INT	-116.15	-51.82	-9.83	-14.89	-192.69

TABLE IV: Energy decomposition analysis of the many-body expansion of the strongly-bound, radical, cationic COM1 complex from Bell et al.[59] in kJ/mol. E_2 and E_3 denote two- and three-body terms in the expansion. A, W, and F indicate the vinyl alcohol radical cation, water, and formaldehyde, respectively.

The two-body term between the vinyl alcohol radical cation (A) and formaldehyde (F), E_2[AF], describes primarily the electrostatic interaction between the cation and favorably aligned dipole of formaldehyde with minor additional stabilization from POL and even less from DISP. Compared to the other two-body terms, repulsive PAULI and attractive CT contributions are very small in magnitude for E_2[AF] due to the large distance between these two monomers.

The two-body term between water (W) and formaldehyde (F), E_2[WF], is the weakest as it involves no permanent monopoles. The hydrogen bond length in this case is slightly compressed ($R_{O\text{-}H}$ = 1.75 Å) compared to the ωB97M-V/def2-QZVPPD optimal bond length ($R_{O\text{-}H}$ = 2.02 Å). While not optimal for this pair interaction, it is optimal for the cluster as a whole within the model chemistry of the original work.[59] The consequence of this shorter bond is a fairly repulsive PAULI term and larger magnitude stabilizing interactions across the board relative to an equilibrium water-formaldehyde interaction, though, by definition, they do not quite match the energy increase due to Pauli repulsion.

The three-body term, E_3[AWF], is, as in our past analysis[59], dominated by POL and CT contributions owing to the presence of multiple permanent moments and to the concerted charge donation from formaldehyde to water to the vinyl alcohol radical cation. Classical electrostatic interactions are pairwise additive; however, our electrostatic term accounts for the non-additive density deformations accompanying the formation of the initial supersystem wavefunction, and so the three-body electrostatic term is not explicitly zero though in this case it is quite small (as are PAULI and DISP).

IV. CONCLUSIONS

We have introduced a second generation ALMO-EDA with the following key properties:

1. The EDA can work with any single determinant Kohn-Sham density functional theory model chemistry including the exact functional.

2. It produces physically meaningful terms with correct sign and asymptotic behavior provided that appropriate pairs of functionals are chosen. Each term has a stable complete basis set limit that remains physically valid.

3. It is maximally descriptive. The EDA further divides the frozen interaction into electrostatic, Pauli and dispersion contributions without the difficulties of the common separation into classical electrostatics and a Pauli term that is contaminated with some attractive contributions in calculations using modern functionals.

4. The EDA is variational and optionally fully variational for extremely strong interactions where removal of constant density polarization[40] from the initial supersystem wavefunction is necessary.

Together with state-of-the-art density functionals that are capable of accurately describing noncovalent interaction, this new ALMO-EDA scheme can be a useful and reliable tool for understanding the often complex interplay of physical contributions to intermolecular binding. In this work, we have employed this new EDA to analyze several different intermolecular interactions including an anti-electrostatic hydrogen bond, which we revealed to be a balance of several contributions and not as counterintuitive or surprising as the name might suggest. The examination of two configurations of the adenine-thymine complex demonstrated that our EDA is capable of discerning between two qualitatively different types of interactions, made possible in large part by the new decomposition of the frozen energy. Competition between the stabilizing frozen interactions (permanent electrostatics and dispersion) and orbital interactions (polarization and charge transfer) also emerges as the key factor determining the relative energies of complexes between Cl^- and 1,3-dimethyl imidazolium cation, which are differently ordered than for Cl^- and s-triazine. Finally, in our analysis of the ionized glycerol complex, we demonstrated the utility of the combination of many-body expansions and EDA, and, taking advantage of the additional information provided by the newly added ELEC, PAULI, and DISP terms, we enhanced our previous description of this interaction while validating the earlier computational protocol.

V. ACKNOWLEDGEMENTS

This work was supported by a grant (CHE-1363342) from the U.S. National Science Foundation.

[1] M. J. S. Phipps, T. Fox, C. S. Tautermann, and C.-K. Skylaris, Chem. Soc. Rev. **44**, 3177 (2015).
[2] P. R. Horn and M. Head-Gordon, J. Chem. Phys. **143**, 114111 (2015).
[3] J. Klimes and A. Michaelides, J. Chem. Phys. **137**, 120901 (2012).
[4] R. A. DiStasio Jr., V. V. Gobre, and A. Tkatchenko, J. Phys.: Condens. Matter **26**, 213202 (2014).
[5] C. Corminboeuf, Acc. Chem. Res. **47**, 3217 (2014).
[6] J. P. Wagner and P. R. Schreiner, Ang. Chem. Int. Ed. **54**, 12274 (2015).
[7] S. Grimme, J. Comput. Chem. **27**, 1787 (2006).
[8] S. Grimme, J. Antony, S. Ehrlich, and H. Krieg, J. Chem. Phys. **132**, 154104 (2010).
[9] O. A. Vydrov and T. Van Voorhis, J. Chem. Phys. **133**, 244103 (2010).
[10] K. Berland, V. R. Cooper, K. Lee, E. Schroeder, T. Thonhauser, P. Hyldgaard, and B. I. Lundqvist, Rep. Prog. Phys. **78**, 066501 (2015).
[11] J. D. Chai and M. Head-Gordon, J. Chem. Phys. **128**, 084106 (2008).
[12] N. Mardirossian and M. Head-Gordon, Phys. Chem. Chem. Phys. **16**, 9904 (2014).
[13] N. Mardirossian and M. Head-Gordon, J. Chem. Phys. **142** (2015).
[14] N. Mardirossian and M. Head-Gordon, J. Chem. Phys. , (in press, 2016) (2016).
[15] K. Kitaura and K. Morokuma, Int. J. Quantum Chem. **10**, 325 (1976).
[16] K. Morokuma, Acc. Chem. Res. **10**, 294 (1977).
[17] W. Chen and M. S. Gordon, J. Phys. Chem. **100**, 14316 (1996).
[18] T. Ziegler and A. Rauk, Theor. Chem. Acc. **46**, 1 (1977).
[19] T. Ziegler and A. Rauk, Inorg. Chem. **18**, 1558 (1979).
[20] M. P. Mitoraj, A. Michalak, and T. Ziegler, J. Chem. Theory Comput. **5**, 962 (2009).
[21] F. M. Bickelhaupt and E. J. Baerends, in *Reviews in Computational Chemistry*, Vol. 15, edited by K. B. Lipkowitz and D. B. Boyd (John Wiley & Sons, Inc., New York, 2007) Chap. 1, pp. 1–86.
[22] A. Krapp, F. M. Bickelhaupt, and G. Frenking, Chem. Eur. J. **12**, 9196 (2006).
[23] M. von Hopffgarten and G. Frenking, WIREs Comput. Mol. Sci. **2**, 43 (2012).
[24] R. Z. Khaliullin, E. A. Cobar, R. C. Lochan, A. T. Bell, and M. Head-Gordon, J. Phys. Chem. A **111**, 8753 (2007).
[25] R. Z. Khaliullin, A. T. Bell, and M. Head-Gordon, J. Chem. Phys. **128**, 184112 (2008).
[26] P. R. Horn, E. J. Sundstrom, T. A. Baker, and M. Head-Gordon, J. Chem. Phys. **138**, 134119 (2013).
[27] Y. Mo, J. Gao, and S. D. Peyerimhoff, J. Chem. Phys. **112**, 5530 (2000).
[28] Y. Mo, L. Song, and Y. Lin, J. Phys. Chem. A **111**, 8291 (2007).
[29] Y. Mo, P. Bao, and J. Gao, Phys. Chem. Chem. Phys. **13**, 6760 (2011).
[30] S. N. Steinmann, C. Corminboeuf, W. Wu, and Y. Mo, J. Phys. Chem. A **115**, 5467 (2011).
[31] H. Stoll, G. Wagenblast, and H. Preuß, Theor. Chem. Acc. **57**, 169 (1980).
[32] E. Gianinetti, M. Raimondi, and E. Tornaghi, Int. J. Quantum Chem. **60**, 157 (1996).
[33] R. Z. Khaliullin, M. Head-Gordon, and A. T. Bell, J. Chem. Phys. **124**, 204105 (2006).
[34] J. Thirman and M. Head-Gordon, J. Chem. Phys. **143**, 084124 (2015).
[35] R. J. Azar, P. R. Horn, E. J. Sundstrom, and M. Head-Gordon, J. Chem. Phys. **138**, 084102 (2013).
[36] K. U. Lao and J. M. Herbert, J. Chem. Theory Comput. **12**, 2569 (2016).
[37] Q. Wu, P. W. Ayers, and Y. Zhang, J. Chem. Phys. **131**, 164112 (2009).
[38] Q. Wu, J. Chem. Phys. **140**, 244109 (2014).
[39] J. Řezáč and A. de la Lande, J. Chem. Theory Comput. **11**, 528 (2015).
[40] P. R. Horn and M. Head-Gordon, J. Chem. Phys. **144**, 084118 (2016).
[41] E. D. Glendening and A. Streitwieser, J. Chem. Phys. **100**, 2900 (1994).
[42] G. K. Schenter and E. D. Glendening, J. Phys. Chem. **100**, 17152 (1996).

[43]E. D. Glendening, J. Phys. Chem. A **109**, 11936 (2005).
[44]A. Reed and F. Weinhold, J. Chem. Phys. **78**, 4066 (1983).
[45]A. E. Reed, L. A. Curtiss, and F. Weinhold, Chem. Rev. **88**, 899 (1988).
[46]S. Rybak, B. Jeziorski, and K. Szalewicz, J. Chem. Phys. **95**, 6576 (1991).
[47]B. Jeziorski, R. Moszynski, and K. Szalewicz, Chem. Rev. **94**, 1887 (1994).
[48]A. J. Misquitta, B. Jeziorski, and K. Szalewicz, Phys. Rev. Lett. **91**, 033201 (2003).
[49]A. J. Misquitta, R. Podeszwa, B. Jeziorski, and K. Szalewicz, J. Chem. Phys. **123**, 214103 (2005).
[50]I. C. Hayes and A. J. Stone, Mol. Phys. **53**, 83 (1984).
[51]P. S. Zuchowski, R. Podeszwa, R. Moszyinski, B. Jeziorski, and K. Szalewicz, J. Chem. Phys. **129**, 084101 (2008).
[52]A. J. Stone and A. J. Misquitta, Chem. Phys. Lett. **473**, 201 (2009).
[53]A. J. Misquitta, J. Chem. Theory Comput. **9**, 5313 (2013).
[54]F. Weinhold and R. A. Klein, Ang. Chem. Int. Ed. **53**, 11214 (2014).
[55]G. Frenking and G. F. Caramori, Ang. Chem. Int. Ed. **54**, 2596 (2015).
[56]F. Weinhold and R. A. Klein, Ang. Chem. Int. Ed. **54**, 2600 (2015).
[57]P. Jurecka, J. Sponer, J. Cerný, and P. Hobza, Phys. Chem. Chem. Phys. **8**, 1985 (2006).
[58]R. Matthews, T. Welton, and P. Hunt, Phys. Chem. Chem. Phys. **16**, 3238 (2014).
[59]F. Bell, Q. N. Ruan, A. Golan, P. R. Horn, M. Ahmed, S. R. Leone, and M. Head-Gordon, J. Am. Chem. Soc. **135**, 14229 (2013).
[60]P. R. Horn, Y. Mao, and M. Head-Gordon, J. Chem. Phys. **144**, 114107 (2016).
[61]K. Pernal, R. Podeszwa, K. Patkowski, and K. Szalewicz, Phys. Rev. Lett. **103**, 263201 (2009).
[62]Y. Zhang and W. Yang, Phys. Rev. Lett. **80**, 890 (1998).
[63]E. Gianinetti, A. Vandoni, A. Famulari, and M. Raimondi, Adv. Quantum Chem. **31**, 251 (1998).
[64]T. Nagata, O. Takahashi, K. Saito, and S. Iwata, J. Chem. Phys. **115**, 3553 (2001).
[65]Y. Shao, L. F. Molnar, Y. Jung, J. Kussmann, C. Ochsenfeld, S. T. Brown, A. T. B. Gilbert, L. V. Slipchenko, S. V. Levchenko, D. P. O'Neill, R. A. DiStasio, R. C. Lochan, T. Wang, G. J. O. Beran, N. A. Besley, J. M. Herbert, C. Y. Lin, T. Van Voorhis, S. H. Chien, A. Sodt, R. P. Steele, V. A. Rassolov, P. E. Maslen, P. P. Korambath, R. D. Adamson, B. Austin, J. Baker, E. F. C. Byrd, H. Dachsel, R. J. Doerksen, A. Dreuw, B. D. Dunietz, A. D. Dutoi, T. R. Furlani, S. R. Gwaltney, A. Heyden, S. Hirata, C.-P. Hsu, G. Kedziora, R. Z. Khalliulin, P. Klunzinger, A. M. Lee, M. S. Lee, W. Liang, I. Lotan, N. Nair, B. Peters, E. I. Proynov, P. A. Pieniazek, Y. M. Rhee, J. Ritchie, E. Rosta, C. D. Sherrill, A. C. Simmonett, J. E. Subotnik, H. L. Woodcock, W. Zhang, A. T. Bell, A. K. Chakraborty, D. M. Chipman, F. J. Keil, A. Warshel, W. J. Hehre, H. F. Schaefer, J. Kong, A. I. Krylov, P. M. W. Gill, and M. Head-Gordon, Phys. Chem. Chem. Phys. **8**, 3172 (2006).
[66]Y. Shao, Z. Gan, E. Epifanovsky, A. T. Gilbert, M. Wormit, J. Kussmann, A. W. Lange, A. Behn, J. Deng, X. Feng, D. Ghosh, M. Goldey, P. R. Horn, L. D. Jacobson, I. Kaliman, R. Z. Khaliullin, T. Kuś, A. Landau, J. Liu, E. I. Proynov, Y. M. Rhee, R. M. Richard, M. A. Rohrdanz, R. P. Steele, E. J. Sundstrom, H. L. Woodcock, P. M. Zimmerman, D. Zuev, B. Albrecht, E. Alguire, B. Austin, G. J. O. Beran, Y. A. Bernard, E. Berquist, K. Brandhorst, K. B. Bravaya, S. T. Brown, D. Casanova, C.-M. Chang, Y. Chen, S. H. Chien, K. D. Closser, D. L. Crittenden, M. Diedenhofen, R. A. DiStasio, H. Do, A. D. Dutoi, R. G. Edgar, S. Fatehi, L. Fusti-Molnar, A. Ghysels, A. Golubeva-Zadorozhnaya, J. Gomes, M. W. Hanson-Heine, P. H. Harbach, A. W. Hauser, E. G. Hohenstein, Z. C. Holden, T.-C. Jagau, H. Ji, B. Kaduk, K. Khistyaev, J. Kim, J. Kim, R. A. King, P. Klunzinger, D. Kosenkov, T. Kowalczyk, C. M. Krauter, K. U. Lao, A. Laurent, K. V. Lawler, S. V. Levchenko, C. Y. Lin, F. Liu, E. Livshits, R. C. Lochan, A. Luenser, P. Manohar, S. F. Manzer, S.-P. Mao, N. Mardirossian, A. V. Marenich, S. A. Maurer, N. J. Mayhall, E. Neuscamman, C. M. Oana, R. Olivares-Amaya, D. P. O'Neill, J. A. Parkhill, T. M. Perrine, R. Peverati, A. Prociuk, D. R. Rehn, E. Rosta, N. J. Russ, S. M. Sharada, S. Sharma, D. W. Small, A. Sodt, T. Stein, D. Stück, Y.-C. Su, A. J. Thom, T. Tsuchimochi, V. Vanovschi, L. Vogt, O. Vydrov, T. Wang, M. A. Watson, J. Wenzel, A. White, C. F. Williams, J. Yang, S. Yeganeh, S. R. Yost, Z.-Q. You, I. Y. Zhang, X. Zhang, Y. Zhao, B. R. Brooks, G. K. Chan, D. M. Chipman, C. J. Cramer, W. A. Goddard, M. S. Gordon, W. J. Hehre, A. Klamt, H. F. Schaefer, M. W. Schmidt, C. D. Sherrill, D. G. Truhlar, A. Warshel, X. Xu, A. Aspuru-Guzik, R. Baer, A. T. Bell, N. A. Besley, J.-D. Chai, A. Dreuw, B. D. Dunietz, T. R. Furlani, S. R. Gwaltney, C.-P. Hsu, Y. Jung, J. Kong, D. S. Lambrecht, W. Liang, C. Ochsenfeld, V. A. Rassolov, L. V. Slipchenko, J. E. Subotnik, T. Van Voorhis, J. M. Herbert, A. I. Krylov, P. M. Gill, and M. Head-Gordon, Mol. Phys. **113**, 184 (2015).
[67]D. Rappoport and F. Furche, J. Chem. Phys. **133**, 134105 (2010).
[68]A. D. Becke, Phys. Rev. A **38**, 3098 (1988).
[69]C. Lee, W. Yang, and R. G. Parr, Phys. Rev. B **37**, 785 (1988).
[70]A. D. Becke, J. Chem. Phys. **98**, 5648 (1993).
[71]R. Z. Khaliullin, A. T. Bell, and M. Head-Gordon, Chem. Eur. J. **15**, 851 (2009).
[72]M. S. Marshall, L. A. Burns, and C. D. Sherrill, J. Chem. Phys. **135**, 194102 (2011).
[73]W. Gamrad, A. Dreier, R. Goddard, and K. Porschke, Angew. Chem. Int. Ed. **54**, 4482 (2015).
[74]A. Knorr, P. Stange, K. Fumino, F. Weinhold, and R. Ludwig, ChemPhysChem **17**, 458 (2016).
[75]F. Weinhold and R. A. Klein, Chem. Educ. Res. Pract. **15**, 276 (2014).
[76]I. Mata, E. Molins, I. Alkorta, and E. Espinosa, J. Phys. Chem. A **119**, 183 (2015).
[77]F. Weinhold and J. E. Carpenter, J. Mol. Struct. THEOCHEM **165**, 189 (1988).
[78]M. Giese, M. Albrecht, and K. Rissanen, Chem. Comm. **52**, 1778 (2016).
[79]O. B. Berryman, V. S. Bryantsev, D. P. Stay, D. W. Johnson, and B. P. Hay, J. Am. Chem. Soc. **129**, 48 (2007).
[80]R. Matthews, T. Welton, and P. Hunt, Phys. Chem. Chem. Phys. **17**, 14437 (2015).
[81]P. Hunt, C. Ashworth, and R. Matthews, Chem. Soc. Rev. **44**, 1257 (2015).